
ADVANCED
HEALTHCARE
MATERIALS

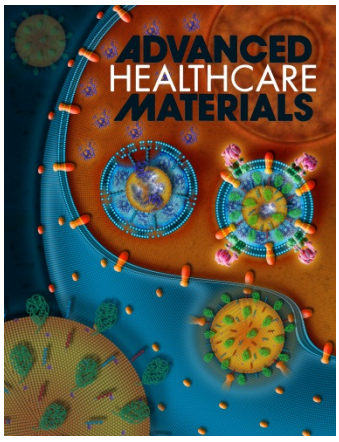

Mesoporous silica nanoparticle-supported lipid bilayers, or 'protocells', are loaded with ricin toxin A-chain (RTA) and targeted to hepatocellular carcinoma (HCC) with a peptide (SP94) that binds to unknown HCC surface antigen(s). RTA-loaded, SP94-targeted protocells are selectively internalized by HCC via receptor-mediated endocytosis and release encapsulated RTA upon endosome acidification. An endosomolytic peptide (H5WYG), present on the protocell's supported lipid bilayer, disrupts endosomal membranes via the proton-sponge mechanism, thereby releasing RTA into the cytosol of HCC cells. As described by Eric Carnes and co-workers, RTA-loaded, SP94-targeted protocells kill HCC at a RTA concentration of 30 pM without affecting the viability of non-cancerous cells.

In the cover image, protocells modified with SP94 (red), H5WYG (blue), and PEG (green) are shown interacting with an HCC cell.

Delivery of Ricin Toxin A-Chain by Peptide-Targeted Mesoporous Silica Nanoparticle-Supported Lipid Bilayers

Katharine Epler, David Padilla, Genevieve Phillips, Peter Crowder, Robert Castillo, Dan Wilkinson, Brian Wilkinson, Cameron Burgard, Robin Kalinich, Jason Townson, Bryce Chackerian, Cheryl Willman, David Peabody, Walker Wharton, C. Jeffrey Brinker, Carlee Ashley, and Eric Carnes**

There has been a significant effort to utilize protein toxins, including diphtheria, cholera, and ricin toxins, as anti-cancer agents since they are immune to multi-drug resistance mechanisms and are equally active during all phases of the cell cycle.[1] In their natural forms, protein toxins generally consist of three domains: a binding domain that promotes attachment of the toxin to the cell surface, a translocation domain responsible for internalization, and an active domain that ultimately induces cell death by inhibiting intracellular protein synthesis.[2] For example, ricin toxin, found in the seeds of castor oil plants (*Ricinus communis*), is a heterodimer composed of two subunits, A and B, bridged by disulfide bonds. The B subunit mediates entry into cells via receptor-mediated endocytosis, while the A subunit inhibits protein synthesis by cleaving a specific glycosidic bond in 28S ribosomal RNA.[3] To generate cancer-specific cytotoxins, the active domain of protein toxins can be fused to an antibody that promotes specific binding to target cell(s), as well as appropriate intracellular trafficking.[4,5] Catalytically-active ricin toxin A-chain (RTA) has been employed in tumor-specific immunotoxins that inhibit the growth of cancer cells in multiple model systems.[6,7] However, despite the promising activity that immunotoxins have shown in some cases, significant issues remain.[8] Irreconcilable shortcomings frequently result from the generation of an immune response against either the antibody or the toxin, which limits the number of possible treatment cycles. This dosage restriction often prevents the patient from receiving the concentration of toxin necessary to successfully eradicate cancerous cells, especially when they exist in tumor form.[2] Improved delivery systems that overcome these limitations would expand the clinical utility of this potentially valuable class of biologically-active reagents.

We recently reported development of the mesoporous silica nanoparticle-supported lipid bilayer, or "protocell",[9,10] a highly versatile nanocarrier that synergistically combines features of liposomes and mesoporous silica nanoparticles[11–21] and, therefore, possesses many characteristics of an ideal targeted delivery platform. The high pore volume and surface area of the spherical, porous silica nanoparticle core enable encapsulation of high concentrations of disparate therapeutic molecules, including low molecular weight drugs, small interfering RNA

Dr. E. Carnes
Department of Chemical Engineering
University of New Mexico
1 University of New Mexico
MSC 01-1120, Albuquerque, NM 87131, USA
Fax: (505) 272-7336
E-mail: eccarne@unm.edu

Dr. C. Ashley
Biotechnology and Bioengineering Department
Sandia National Laboratories
P.O. Box 969, MS 9292, Livermore, CA 94551, USA
Fax: (925) 294-3020
E-mail: ceashle@sandia.gov

K. Epler, D. Padilla, R. Castillo, D. Wilkinson, B. Wilkinson, C. Burgard, Dr. J. Townson, Dr. C. J. Brinker
Center for Micro-Engineered Materials
University of New Mexico
1 University of New Mexico
MSC 01-1120, Albuquerque, NM 87131, USA

G. Phillips, Dr. B. Chackerian, Dr. C. Willman, Dr. D. Peabody, Dr. W. Wharton, Dr. C. Ashley, Dr. E. Carnes
University of New Mexico Cancer Center
1 University of New Mexico
MSC 07-4025, Albuquerque, NM 87131, USA

P. Crowder, Dr. C. J. Brinker
Department of Chemical Engineering
University of New Mexico
1 University of New Mexico
MSC 01-1120, Albuquerque, NM 87131, USA

R. Kalinich, K. Epler
Ceramic Processing and Inorganic Materials Department
Sandia National Laboratories
P.O. Box 5800, MS 1349, Albuquerque, NM 87185, USA

Dr. B. Chackerian, Dr. D. Peabody, Dr. C. J. Brinker
Department of Molecular Genetics and Microbiology
University of New Mexico Health Sciences Center
1 University of New Mexico
MSC 08-4660, Albuquerque, NM 87131, USA

Dr. C. Willman, Dr. W. Wharton
Department of Pathology
University of New Mexico Health Sciences Center
1 University of New Mexico
MSC 08-4640, Albuquerque, NM 87131, USA

Dr. C. J. Brinker
Self-Assembled Materials Department
Sandia National Laboratories
P.O. Box 5800, MS 1349, Albuquerque, NM 87185, USA

DOI: 10.1002/adhm.201200022

ADVANCED HEALTHCARE MATERIALS
www.advhealthmat.de

Materials Views
www.MaterialsViews.com

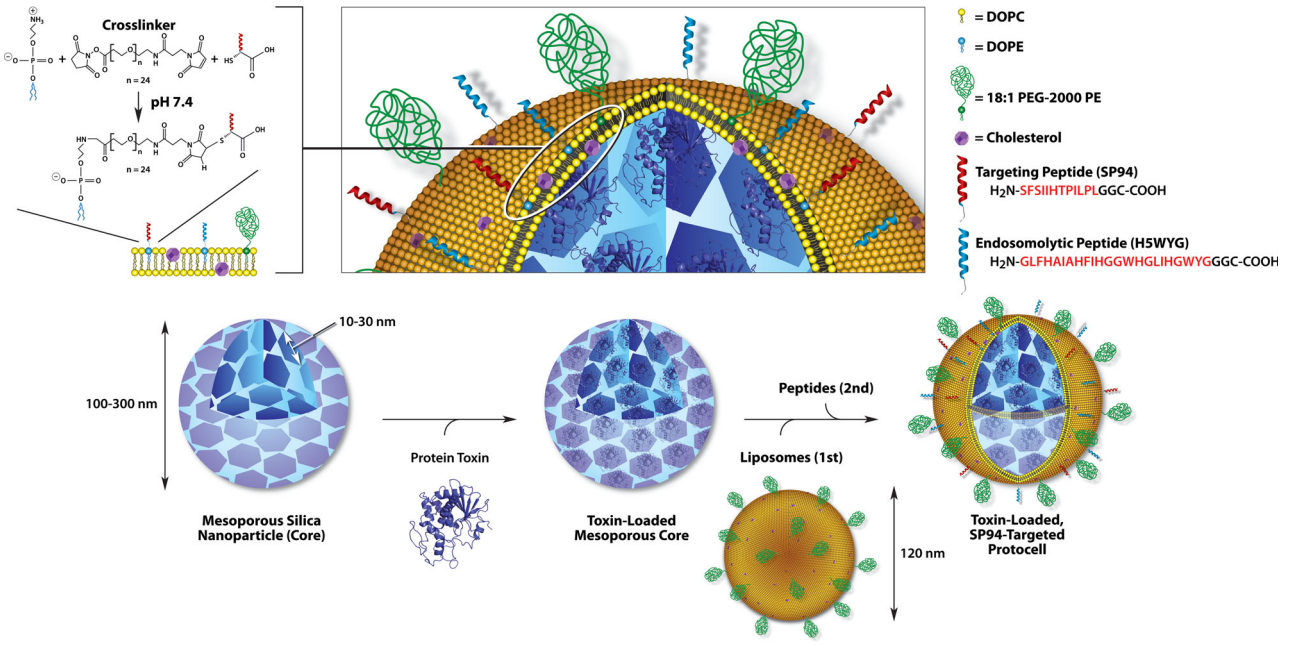

Scheme 1. Schematic depicting the process used to synthesize protein toxin-loaded mesoporous silica nanoparticle-supported lipid bilayers (protocells). To form protocells loaded with a protein toxin and targeted to hepatocellular carcinoma (HCC), mesoporous silica nanoparticles modified with an amine-containing silane (AEPTMS) were first soaked in a solution of a deglycosylated ricin toxin A-chain (RTA). Liposomes composed of DOPC, DOPE, cholesterol, and 18:1 PEG-2000 PE (55:5:30:10 mass ratio) were then fused to toxin-loaded cores. The resulting supported lipid bilayer (SLB) was modified with a targeting peptide (SP94) that binds to HCC and an endosomolytic peptide (H5WYG) that promotes endosomal escape of internalized protocells. Peptides, modified with glycine-glycine (GG) spacers and C-terminal cysteine residues, were conjugated to primary amines present in DOPE moieties via a heterobifunctional crosslinker (SM(PEG)$_{24}$) with a 9.5-nm polyethylene glycol (PEG) spacer. The SP94 and H5WYG sequences reported by Lo *et al.*[29] and Moore *et al.*[25] are given in red.

(siRNA), and protein toxins. Fusion of PEGylated liposomes to cargo-loaded cores results in a supported lipid bilayer (SLB) that prevents premature cargo release, improves colloidal stability, and reduces uptake by innate immune cells. Furthermore, conjugation of targeting and endosomolytic peptides to the SLB allows for cell-specific binding and internalization, as well as cytosolic delivery of encapsulated therapeutic agents. We previously reported that protocells, when loaded with a cocktail of chemotherapeutic drugs and targeted to hepatocellular carcinoma (HCC), induce cytotoxicity at particle:cell ratios as low as one, representing a 10^6-fold improvement over corresponding liposomes.[10] Here we describe high-capacity loading and cell-specific delivery of RTA to HCC via peptide-targeted protocells. As we will demonstrate, protocells address many of the issues that currently limit the clinical use of protein toxins and other macromolecular agents.

As depicted in **Scheme 1**, toxin-loaded, peptide-targeted protocells are formed by first soaking mesoporous silica nanoparticles with large, surface-accessible pores in a solution of RTA. Mesoporous silica nanoparticles were synthesized using an emulsion processing technique originally described by Carroll *et al.*[22] and were subjected to size-exclusion chromatography before being loaded with RTA. Resulting particles had an average diameter of 190-nm and were characterized by a Brunauer-Emmett-Teller (BET) surface area of 850 m^2/g, a pore volume fraction of ~65%, and a bimodal pore morphology composed of 10-30 nm pores interconnected by 2–4 nm pores (see **Figure 1**). RTA-loaded cores were then fused with liposomes composed of a fluid, zwitterionic phospholipid (1,2-dioleoyl-*sn*-glycero-3-phosphocholine, or DOPC; T_m = –20 °C) with 5 wt% 1,2-dioleoyl-*sn*-glycero-3-phosphoethanolamine (DOPE), 30 wt% cholesterol, and 10 wt% 1,2-dioleoyl-*sn*-glycero-3-phosphoethanolamine-N-[methoxy(polyethylene glycol)-2000] (18:1 PEG-2000 PE); cholesterol and PEG-2000 enhance SLB and colloidal stability, respectively, and together reduce non-specific binding to hepatocytes and other control cells (see Supplementary Figures 5 and 7 from *Nat. Mater.* **2011**, *10*, 389[10]), while DOPE moieties provide sites for chemical conjugation of peptides with C-terminal cysteine residues via the amine-to-sulfhydryl heterobifunctional crosslinker, SM(PEG)$_{24}$. Control RTA-loaded liposomes with an identical bilayer composition were prepared as described in the Supporting Information section; we decided to use liposomes as the benchmark against which to judge the performance of RTA-loaded protocells since liposomes have a surface that is comparable to the protocell SLB and have been employed to deliver protein toxins to cancer in order to address limitations of immunotoxins.[23,24]

The capacities and release profiles of RTA-loaded protocells are compared to those of RTA-loaded liposomes in **Figure 2**. As demonstrated by Figure 2a, 10^{12} DOPC liposomes encapsulate ~40 pmol of RTA. In contrast, DOPC protocells with unmodified silica cores (ζ = –25 mV in 0.5 X PBS, pH 7.4) have a nearly 100-fold higher capacity for RTA, and modification of the cores with the amine-containing silane, 3-[2-(2-aminoethylamino) ethylamino]propyltrimethoxysilane (AEPTMS), increases this capacity by another order of magnitude. Deglycosylated RTA

DOI: 10.1002/adhm.201200022

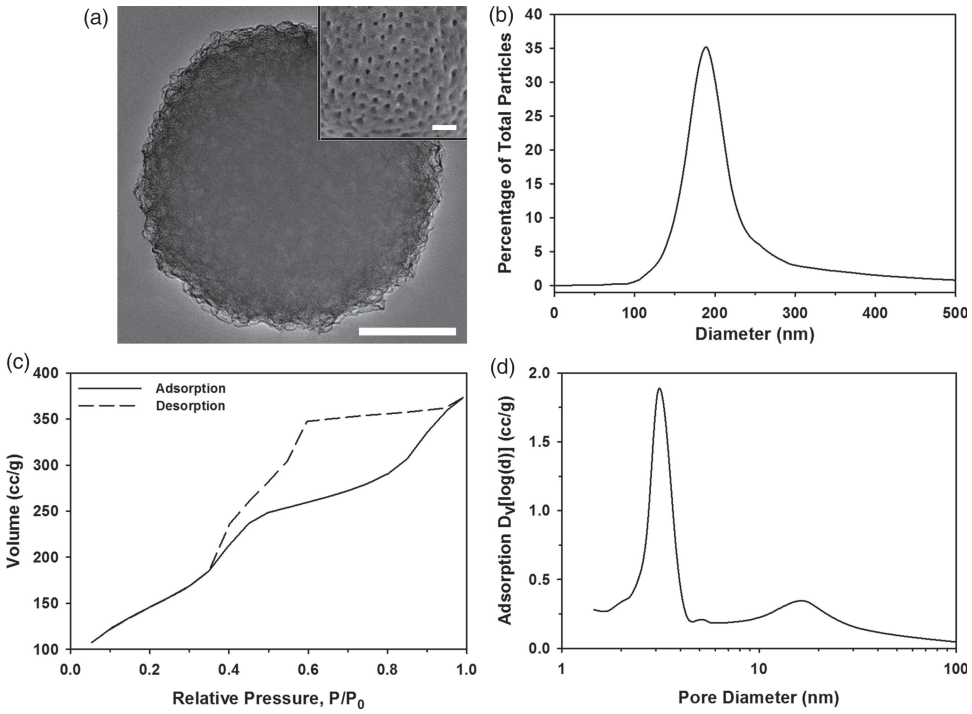

Figure 1. Characterization of the mesoporous silica nanoparticles that form the protocell core. a) Transmission electron microscopy (TEM) image of a bimodal silica particle formed via the emulsion processing technique described by Carroll et al.[22] Scale bar = 50 nm. The inset shows a scanning electron microscopy (SEM) image of a 5-μm bimodal silica particle, in which surface-accessible pores are visible; large particles were used to enhance resolution. Inset scale bar = 200 nm. b) Dynamic light scattering (DLS) of bimodal silica particles after size-exclusion chromatography-based separation. c) Nitrogen adsorption and desorption isotherms for size-separated bimodal particles. The presence of hysteresis is consistent with a network of larger pores interconnected by smaller pores. d) A cumulative pore volume plot, calculated from the adsorption isotherm in (c) using the Barrett-Joyner-Halenda (BJH) model.

has a slight negative charge ($\zeta = -3$ mV) under the conditions used for loading and is, therefore, more efficiently encapsulated within AEPTMS-modified cores ($\zeta = +8$ mV in 0.5 X PBS, pH 7.4) due to attractive electrostatic forces. We selected to use DOPC protocells with AEPTMS-modified cores in all subsequent experiments due to their high capacity for RTA and their low intrinsic cytotoxicity (see Figure S1a). It should be noted that RTA-loaded protocells are slightly larger than RTA-loaded liposomes (205 ± 19.8-nm versus 179 ± 15.1-nm, respectively), resulting in a ~2-fold increase in particle volume. When the capacities shown in Figure 2a are normalized against particle volume, however, DOPC protocells with AEPTMS-modified cores still encapsulate 500-fold more RTA than corresponding DOPC liposomes, which demonstrates that the high-surface-area mesoporous core confers an intrinsic loading capacity that greatly exceeds what might be expected based on volumetric differences alone.

The RTA release profiles of DOPC protocells and liposomes upon exposure to neutral or acidic conditions are shown in Figure 2b and 2c, respectively. When incubated in a simulated body fluid at pH 7.4, DOPC protocells release only ~5% of their encapsulated RTA over the course of 72 hours. When the pH is reduced to reflect conditions in the endosomal/lysosomal pathway, however, DOPC protocells release nearly 100% of their RTA content within 24 hours. We have previously shown that the zeta potential of DOPC protocells approaches that of bare silica cores after exposure to a pH 5.0 buffer for 2 hours (see Supplementary Figure 12 from *Nat. Mater.* **2011**, *10*, 389[10]); this result demonstrates that acidic conditions destabilize the SLB, likely by reducing electrostatic and dipolar interactions between cargo-loaded cores and lipid headgroups in the SLB. We have also shown that AEPTMS-modified cores completely dissolve within 12–24 hours at neutral and mildly acidic pH values (see Supplementary Figure 2 from *Nat. Mater.* **2011**, *10*, 389[10]); we, therefore, postulate that the rate of RTA release from DOPC protocells upon dispersion in a pH 5.0 buffer is initiated by SLB destabilization and is due to both diffusion of RTA from the core's mesopores and dissolution of the core itself. In contrast to DOPC protocells, which stably encapsulate RTA until endosomal-like conditions trigger its release from the core, both DOPC liposomes and AEPTMS-modified silica cores that lack a lipid bilayer coating rapidly lose their encapsulated RTA under neutral and acidic pH conditions. Thus, in terms of capacity, stability, and triggered release, DOPC protocells represent a substantial improvement over liposomes prepared using state-of-the-art techniques.

We have previously shown that modification of the SLB with a low density (0.015 wt%, or ~6 peptides/protocell) of SP94, a peptide that recognizes unknown HCC surface antigen(s), promotes sub-nanomolar affinity for the HCC line, Hep3B, and induces receptor-mediated endocytosis followed by lysosomal processing (see Supplementary Figures 7 and 10 from *Nat. Mater.* **2011**, *10*, 389[10]). We, therefore, hypothesized that DOPC protocells co-modified with SP94 and an endosomolytic peptide

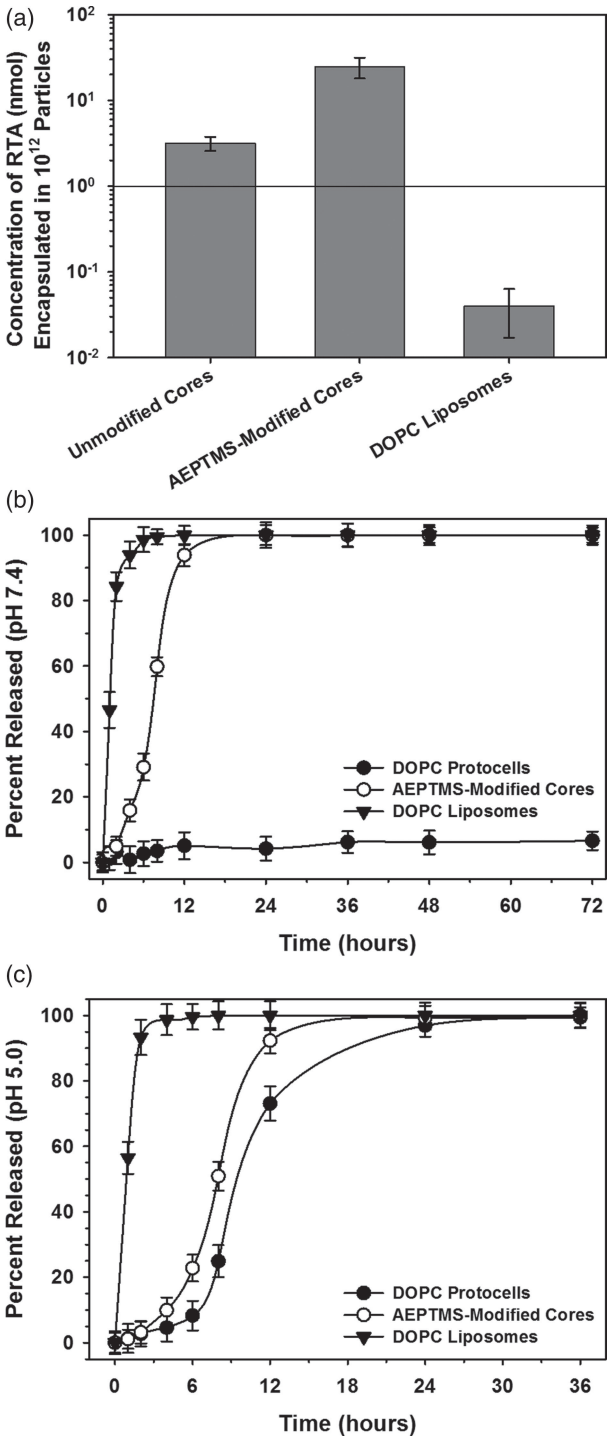

Figure 2. Protocells encapsulate a high concentration of ricin toxin A-chain (RTA), the release of which is triggered by acidic pH. a) The concentrations of RTA that can be encapsulated within DOPC protocells with unmodified silica cores, DOPC protocells with AEPTMS-modified silica cores, and DOPC liposomes. b, c) Time-dependent release of RTA upon exposure of DOPC protocells with AEPTMS-modified cores and DOPC liposomes to a pH 7.4 simulated body fluid (b) or a pH 5.0 buffer (c) at 37°C. Release of RTA from AEPTMS-modified cores that lack supported lipid bilayers is included for comparison. The protocell and liposome concentrations were maintained at 10^{12} particles/mL in all experiments. Error bars represent 95% confidence intervals (1.96 σ) for n = 3.

(H5YWG) that disrupts endosomal membranes via the proton-sponge mechanism[25] should selectively deliver RTA, which is especially cytotoxic but sensitive to lysosomal degradation, to Hep3B in doses sufficient for effective induction of apoptosis. **Figure 3** demonstrates that RTA-loaded, SP94-targeted protocells inhibit nascent protein synthesis and induce apoptosis in Hep3B at picomolar concentrations of RTA. Figure 3a shows dose-response curves for RTA-loaded protocells, RTA-loaded liposomes, and free RTA. Protocells induce half-maximal inhibition of protein synthesis (IC_{50}) at ~5 pM of RTA, a concentration that is 100-fold and 3500-fold less than the IC_{50} values of RTA-loaded liposomes and free RTA, respectively (see Table S1). Figure 3b demonstrates the effects of incubating Hep3B with 30 pM of RTA, the concentration required to repress 90% of protein biosynthesis (IC_{90}) when delivered via SP94-targeted protocells. At this concentration, RTA-loaded protocells cause a 50% reduction in nascent protein synthesis within ~24 hours and complete repression within 60 hours. In contrast, RTA-loaded liposomes repress protein biosynthesis by only 10% over the course of 5 days, a result that is nearly indistinguishable from the effect of free RTA.

The ability of RTA-loaded protocells to selectively kill Hep3B but not control hepatocytes is demonstrated by Figure 3c and 3d. RTA-loaded, SP94-targeted protocells induce apoptosis, as measured by activation of caspase-9 and caspase-3, in 50% of Hep3B by 20–28 hours at a RTA concentration of 30 pM, with complete cell death occurring by 48 hours. The cytotoxicity of RTA-loaded protocells depends on the presence of both SP94 and the endosomolytic peptide, however (see Figure S1); in the absence of H5WYG, RTA-loaded protocells kill only 15% of Hep3B. As demonstrated by Figure 3c and 3d, hepatocyte viability is unaffected by RTA-loaded, SP94-targeted protocells, even after 5 days of incubation, a result that is confirmed by the representative confocal fluorescence microscopy images shown in Figure S2 and S3. In contrast, as shown by the left axis of Figure 3d, RTA-loaded, SP94-targeted liposomes fail to induce apoptosis of Hep3B at a RTA concentration of 30 pM. Furthermore, as shown by the right axis of Figure 3d, 10^5-fold more RTA-loaded liposomes are required to induce apoptosis in 90% of Hep3B (LC_{90}), demonstrating that the combined capacity, stability, and targeting efficacy of SP94-targeted protocells enable efficient, cell-specific delivery of RTA.

In conclusion, we have demonstrated that SP94-targeted protocells efficiently package and deliver protein toxins to HCC in a cell-specific fashion and have the potential to address many limitations of state-of-the-art toxin-based therapies.[2,8] 190-nm silica nanoparticles with bimodal porosity can be rapidly loaded with, on average, ~1 × 10^4 RTA molecules per particle, which demonstrates that protocells have a capacity that is sufficient to overcome current dose limits.[7] Fusion of DOPC liposomes to RTA-loaded cores results in the formation of a stable SLB that enables long-term cargo retention under neutral pH conditions (see Figure 2b), reduces non-specific binding to non-target cells (see Supplementary Figures 5 and 7 from *Nat. Mater.* **2011**, *10*, 389[10]), prevents particle aggregation, and is expected to mitigate immunogenicity of encapsulated toxins. Targeting peptides conjugated to the fluid but stable SLB interact multivalently with cell surface receptors and induce receptor-mediated endocytosis of RTA-loaded protocells (see Figure 4 and Supplementary

DOI: 10.1002/adhm.201200022

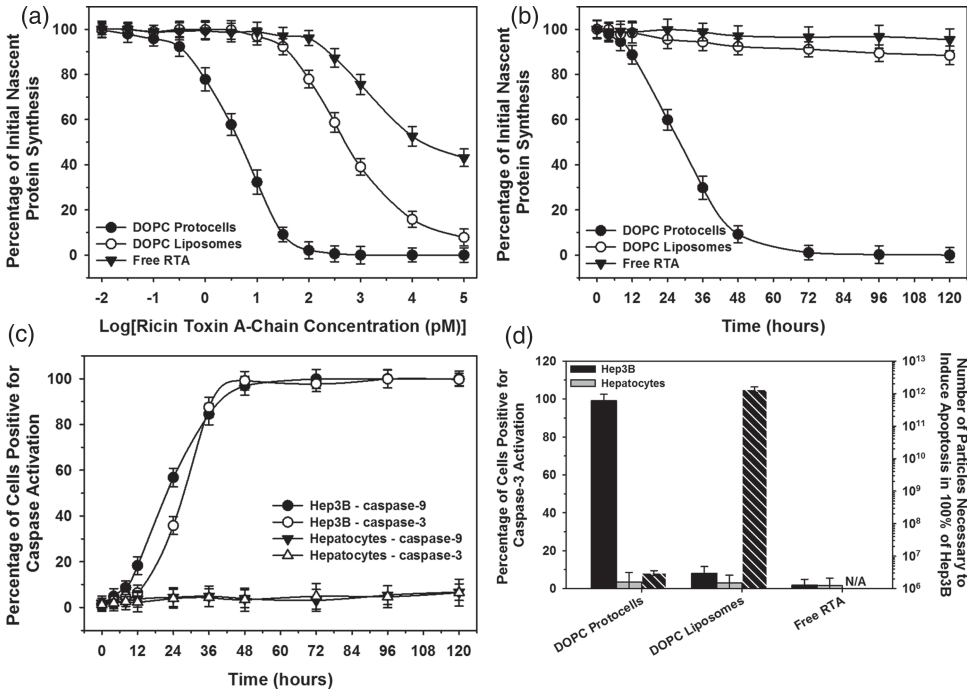

Figure 3. RTA-loaded, SP94-targeted protocells inhibit protein biosynthesis and induce apoptosis in HCC without affecting hepatocyte viability. a,b) Dose (a) and time (b) dependent decreases in nascent protein synthesis upon exposure of Hep3B to RTA-loaded, SP94-targeted protocells; RTA-loaded, SP94-targeted liposomes; or free RTA. 1×10^6 cells were continually exposed to various concentrations of RTA for 48 hours in (a) and to 30 pM of RTA for various periods of time in (b). c) The percentages of 1×10^6 Hep3B and hepatocytes that become positive for caspase-9 or caspase-3 activation upon exposure to RTA-loaded, SP94-targeted protocells for various periods of time at 37 °C. The total RTA concentration was maintained at 30 pM. (d, left axis) The percentages of 1×10^6 Hep3B or heaptocytes that become positive for caspase-3 activation upon exposure to RTA-loaded, SP94-targeted protocells; RTA-loaded, SP94-targeted liposomes; or free RTA for 48 hours at 37 °C. The RTA concentration was maintained at 30 pM. (d, right axis) The number of RTA-loaded, SP94-targeted protocells and liposomes that must be incubated with 1×10^6 Hep3B to induce apoptosis (as measured by caspase-3 activation) in 90% of cells within 48 hours at 37 °C (hatched bar). Protocell and liposome bilayers were composed of DOPC with 5 wt% DOPE, 30 wt% cholesterol, and 10 wt% PEG-2000 and were modified with 0.015 wt% SP94 and 0.500 wt% H5WYG. Error bars represent 95% confidence intervals (1.96 σ) for n = 3.

Table II from *Nat. Mater.* **2011**, *10*, 389[10]). Within the acidified endosomal environment, SLB destabilization along with the endosomolytic activity of the H5WYG peptide collectively result in dispersion of silica cores within the cytoplasm (see Figure 5 and Supplementary Figure 11 from *Nat. Mater.* **2011**, *10*, 389[10]). Combined diffusion and silica core dissolution enable controlled, sustained cargo release for up to 24 hours. The combined capacity, stability, and internalization efficiency of SP94-targeted protocells result in exceptionally low IC_{90} and LC_{90} values, which are between 25 and 100-fold less than reported values for immunotoxins and toxin-loaded liposomes.[24] Importantly, RTA-loaded, SP94-targeted protocells have practically no adverse effects on control hepatocytes, a feature that is critical to enable use of especially cytotoxic proteins in cancer therapy. Finally, based upon the fact that AEPTMS-modified silica nanoparticles readily dissolve under physiological conditions, as well as recent biocompatibility studies conducted with mesoporous silica nanoparticles,[26–28] we expect the *in vivo* biodegradability of protocells to be high, which should limit their gross and histopathological toxicity. Overall, the evidence presented in this manuscript demostrates that protocells are a unique, versatile delivery platform that may enable protein toxin-based therapies to reach their full potential.

Experimental Section

Detailed protocols for all experiments described in this manuscript are in the Supporting Information section.

Supporting Information

Supporting Information is available from the Wiley Online Library or from the author.

Acknowledgements

This work was supported by the NIH/Roadhmp for Medical Research under grant PHS 2 PN2 EY016570B; NCI Cancer Nanotechnology Platform Partnership grant 1U01CA151792-01; the Air Force Office of Scientific Research grant FA 9550-07-1-0054/9550-10-1-0054; the U.S. Department of Energy, Office of Basic Energy Sciences, Division of Materials Sciences and Engineering; and Sandia National Laboratories' Laboratory Directed Research and Development (LDRD) program. C.E.A. was supported by the President Harry S. Truman Fellowship in National Security Science and Engineering at Sandia National Laboratories. We thank Dimiter Petsev and Nick Carroll for their assistance with nanoparticle synthesis, Darren Dunphy for his help with nanoparticle characterization, Mona Aragon for generating the schematics, and

Carol Ashley for performing final edits of the manuscript. Images in this paper were generated in the University of New Mexico Cancer Center Fluorescence Microscopy Facility, supported by NCRR, NSF and NCI as detailed at http://hsc.unm.edu/crtc/microscopy/Facility.html. Data were generated in the Flow Cytometry Shared Resource Center supported by the University of New Mexico Health Sciences Center and the University of New Mexico Cancer Center. Sandia is a multiprogram laboratory operated by Sandia Corporation, a wholly owned subsidiary of Lockheed Martin Company, for the US Department of Energy's National Nuclear Security Administration under contract DE-AC04-94AL85000.

Received: January 26, 2012
Revised: February 15, 2012
Published online:

[1] J. Lord, J. Gould, P. Richardson, R. A. Spooner, R. Wales, L. Roberts, in: P. R. Shewry, S. Gutteridge (Eds.), *Plant Protein Engineering*, Cambridge University Press, **1992**, pp. 269.
[2] I. Pastan, R. Hassan, D. J. FitzGerald, R. J. Kreitman, *Ann. Rev. Med.* **2007**, *58*, 221.
[3] M. J. Lord, N. A. Jolliffe, C. J. Marsden, C. S. C. Pateman, D. C. Smith, R. A. Spooner, P. D. Watson, L. M. Roberts, *Toxicol. Rev.* **2003**, *22*, 53.
[4] R. F. Alderson, R. J. Kreitman, T. Chen, P. Yeung, R. Herbst, J. A. Fox, I. Pastan, *Clin. Cancer Res.* **2009**, *15*, 832.
[5] A. S. Wayne, R. J. Kreitman, H. W. Findley, G. Lew, C. Delbrook, S. M. Steinberg, M. Stetler-Stevenson, D. J. FitzGerald, I. Pastan, *Clin. Cancer Res.* **2010**, *16*, 1894.
[6] L. Herrera, B. Bostrom, L. Gore, E. Sandler, G. Lew, P. G. Schlegel, V. Aquino, V. Ghetie, E. S. Vitetta, J. Schindler, *J. Pediatr. Hematol./Oncol.* **2009**, *31*, 936.
[7] L. Herrera, S. Yarbrough, V. Ghetie, D. B. Aquino, E. S. Vitetta, *Leukemia.* **2003**, *17*, 334.
[8] I. Pastan, R. Hassan, D. J. FitzGerald, R. J. Kreitman, *Nat. Rev. Cancer* **2006**, *6*, 559.
[9] C. E. Ashley, E. C. Carnes, K. E. Epler, D. P. Padilla, G. K. Phillips, R. E. Castillo, D. C. Wilkinson, B. S. Wilkinson, C. A. Burgard, R. M. Kalinich, J. L. Townson, B. Chackerian, C. L. Willman, D. S. Peabody, W. Wharton, C. J. Brinker, *ACS Nano.* DOI: 10.1021/nn204102q.
[10] C. E. Ashley, E. C. Carnes, G. K. Phillips, D. Padilla, P. N. Durfee, P. A. Brown, T. N. Hanna, J. Liu, B. Phillips, M. B. Carter, N. J. Carroll, X. Jiang, D. R. Dunphy, C. L. Willman, D. N. Petsev, D. G. Evans, A. N. Parikh, B. Chackerian, W. Wharton, D. S. Peabody, C. J. Brinker, *Nat. Mater.* **2011**, *10*, 389.
[11] V. Cauda, C. Argyo, T. Bein, *J. Mater. Chem.* **2010**, *20*, 8693.
[12] V. Cauda, C. Argyo, A. Schlossbauer, T. Bein, *J. Mater. Chem.* **2010**, *20*, 4305.
[13] V. Cauda, H. Engelke, A. Sauer, D. Arcizet, C. Bräuchle, J. Rädler, T. Bein, *Nano Lett.* **2010**, *10*, 2484.
[14] V. Cauda, L. Muehistein, B. Onida, T. Bein, *Microporous Mesoporous Mater.* **2009**, *118*, 435.
[15] V. Cauda, A. Schlossbauer, T. Bein, *Microporous Mesoporous Mater.* **2010**, *132*, 60.
[16] C. Hom, J. Lu, M. Liong, H. Luo, Z. Li, J. I. Zink, F. Tamanoi, *Small.* **2010**, *6*, 1185.
[17] M. Liong, J. Lu, M. Kovochich, T. Xia, S. G. Ruehm, A. E. Nel, F. Tamanoi, J. I. Zink, *ACS Nano.* **2008**, *2*, 889.
[18] H. Meng, M. Liong, T. Xia, Z. Li, Z. Ji, J. I. Zink, A. E. Nel, *ACS Nano.* **2010**, *4*, 4539.
[19] H. Meng, M. Xue, T. Xia, Y.-L. Zhao, F. Tamanoi, J. F. Stoddart, J. I. Zink, A. E. Nel, *J. Am. Chem. Soc.* **2010**, *132*, 12690.
[20] A. M. Sauer, A. Schlossbauer, N. Ruthardt, V. Cauda, T. Bein, C. Bra.uchle, *Nano Lett.* **2010**, *10*, 3684.
[21] T. Xia, M. Kovochich, M. Liong, H. Meng, S. Kabehie, S. George, J. I. Zink, A. E. Nel, *ACS Nano* **2009**, *3*, 3273.
[22] N. J. Carroll, S. Pylypenko, P. B. Atanassov, D. N. Petsev, *Langmuir* **2009**, *25*, 13540.
[23] E. Mastrobattista, G. A. Koning, L. van Bloois, A. C. S. Filipe, W. Jiskoot, G. Storm, *J. Biol. Chem.* **2002**, *277*, 27135.
[24] C. J. Provoda, E. M. Stier, K.-D. Lee, *J. Biol. Chem.* **2003**, *278*, 35102.
[25] N. M. Moore, C. L. Sheppard, T. R. Barbour, S. E. Sakiyama-Elbert, *J. Gene Med.* **2008**, *10*, 1134.
[26] X. Huang, L. Li, T. Liu, N. Hao, H. Liu, D. Chen, F. Tang, *ACS Nano* **2011**, *5*, 5390.
[27] J. Lu, M. Liong, Z. Li, J. I. Zink, F. Tamanoi, *Small* **2010**, *6*, 1794.
[28] V. Mamaeva, J. M. Rosenholm, L. T. Bate-Eya, L. Bergman, E. Peuhu, A. Duchanoy, L. E. Fortelius, S. Landor, D. M. Toivola, M. Linden, C. Sahlgren, *Mol. Ther.* **2011**, *19*, 1538.
[29] A. Lo, C.-T. Lin, H.-C. Wu, *Mol. Cancer Ther.* **2008**, *7*, 579.